Three-dimensional direct numerical simulation of a turbulent lifted hydrogen jet flame in heated coflow: a chemical explosive mode analysis

T. F. LU[1]†, C. S. YOO[2]‡, J. H. CHEN[2] AND C. K. LAW[1]¶

[1]Department of Mechanical and Aerospace Engineering, Princeton University, Princeton, NJ 08544, USA

[2]Combustion Research Facility, Sandia National Laboratories, Livermore, CA 94551, USA

A chemical explosive mode analysis (CEMA) was developed as a new diagnostic to identify flame and ignition structure in complex flows. CEMA was then used to analyse the near-field structure of the stabilization region of a turbulent lifted hydrogen–air slot jet flame in a heated air coflow computed with three-dimensional direct numerical simulation. The simulation was performed with a detailed hydrogen–air mechanism and mixture-averaged transport properties at a jet Reynolds number of 11 000 with over 900 million grid points. Explosive chemical modes and their characteristic time scales, as well as the species involved, were identified from the Jacobian matrix of the chemical source terms for species and temperature. An explosion index was defined for explosive modes, indicating the contribution of species and temperature in the explosion process. Radical and thermal runaway can consequently be distinguished. CEMA of the lifted flame shows the existence of two premixed flame fronts, which are difficult to detect with conventional methods. The upstream fork preceding the two flame fronts thereby identifies the stabilization point. A Damköhler number was defined based on the time scale of the chemical explosive mode and the local instantaneous scalar dissipation rate to highlight the role of auto-ignition in affecting the stabilization points in the lifted jet flame.

1. Introduction

Turbulent lifted flames are of relevance to the satisfactory operation of many practical devices. Consequently, there have been extensive theoretical and experimental studies on the stabilization mechanism of lifted flames (e.g. Vanquickenborne & van Tiggelen 1966; Kalghatgi 1984; Pitts 1988; Gordon *et al.* 2007). Several explanations have been proposed based on the notion of premixed and non-premixed flames (Peters & Williams 1983; Upatnieks *et al.* 2004; Joedicke, Peters & Mansour 2005; Chung 2007), auto-ignition (Cabra *et al.* 2002; Markides & Mastorakos 2005) and turbulence–flame interactions (Tacke *et al.* 1998; Joedicke *et al.* 2005; Su, Sun & Mungal 2006). However, the viability of most of the postulations is difficult to scrutinize due to the difficulty in performing joint scalar-velocity measurements in

† Current address: Department of Mechanical Engineering, University of Connecticut, CT 06269-3139, USA

‡ Current address: School of Mechanical and Advanced Materials Engineering, Ulsan National Institute of Science and Technology (UNIST), Ulsan 689-798, Republic of Korea

¶ Email address for correspondence: cklaw@princeton.edu

turbulent reactive flows as well as the dearth of accurate simulation data that reflects the chemical response of key intermediate species to turbulent strain. Moreover, most associated utilities for analysis of such complex reacting flows are not concise.

Direct numerical simulation (DNS) is an information-rich platform for the study of turbulent lifted flames (Yamashita, Shimada & Takeno 1996; Mizobuchi *et al.* 2005; Jimenez & Cuenot 2007) by providing complete information of both the flow and chemistry. Restricted by the high computational cost, fully three-dimensional DNS of lifted hydrogen flames in heated coflow with a detailed kinetic mechanism has not become feasible until recently (Yoo, Sankaran & Chen 2009). However, although a detailed analysis was performed on the flame and flow structure that emerged, it remains a challenge to systematically and comprehensively extract salient information from the massive DNS output using rigorous computational utilities.

In response to this challenge, in the present study DNS results obtained in Yoo *et al.* (2009) were analysed with chemical explosive modes, and an explosion index was defined analogously to the concept of the radical pointer from computational singular perturbation (CSP), developed in the mid 1980s (Lam 1985, 1993; Lam & Goussis 1994; Lam 2007). CSP has been primarily applied in the analysis and reduction of stiff nonlinear ordinary differential equations (ODEs), particularly those involving detailed chemical kinetics. It systematically identifies exhausted fast processes that algebraically relate the fast variables with others. In the past two decades, CSP has been widely adopted in various approaches associated with mechanism reduction, including the identification of quasi-steady state (QSS) species (Massias *et al.* 1999a, 1999b; Lu, Ju & Law 2001; Lu & Law 2008), elimination of unimportant species and reactions (Valorani *et al.* 2006) and stiffness removal (Valorani *et al.* 2005; Goussis & Valorani 2006; Lee *et al.* 2007). It has also been applied to analyse complex laminar flow–chemistry interactions (Valorani, Najm & Goussis 2003), as well as biochemical systems (Goussis & Najm 2006).

As a rigorous method to treat both linear and nonlinear systems with time scale separation, CSP provides a refinement procedure to decouple fast and slow processes iteratively until an arbitrarily high order of accuracy is achieved (Lam & Goussis 1994; Kaper & Kaper 2002; Zagaris, Kaper & Kaper 2004a, 2004b, 2005). In essence, CSP degenerates to the method of intrinsic low-dimensional manifold (Maas & Pope 1992; Ren & Pope 2006, 2007a, 2007b) if the time dependence of the Jacobian is neglected in decoupling the modes. In such cases, eigendecomposition of the Jacobian can be applied instead of the time-consuming refinement procedure (Maas & Pope 1992; Lu *et al.* 2001; Kazakov *et al.* 2006). The eigendecomposition has been found to be sufficiently accurate in many weakly nonlinear applications in mechanism reduction as well as flow simulations. The application of this linearized approach in strongly nonlinear systems however requires careful validation.

In addition to the refinement procedure, CSP provides two important concepts, namely the radical pointer and the participation index (Lam & Goussis 1994), which indicate the involvement of species and reactions, respectively, in the fast processes. In particular, the radical pointer can be employed to identify the candidate species to be solved by algebraic equations. It has also been utilized in the identification of QSS species (Massias *et al.* 1999a, 1999b; Lu *et al.* 2001) and the fast species induced by partial equilibrium reactions (Lu & Law 2008). However, these concepts are not readily applicable to the study of chemical explosive modes, which is important for reactive flows involving ignition processes (Fotache, Kreutz & Law 1997; Kazakov *et al.* 2006).

In the present study, a chemical explosive mode analysis (CEMA) was developed to study the structure and stabilization of a turbulent lifted hydrogen jet flame simulated by DNS. Partially premixed flame fronts in the simulated flow field were unambiguously detected by CEMA. Auto-ignition was further identified as the dominant stabilization mechanism for a lifted hydrogen flame in a heated air coflow aided by this new flame diagnostic. It is, however, important to emphasize at the outset of this study that, while some concepts from CSP were adopted in the formulation of CEMA, this new formulation is mathematically and fundamentally distinctive from CSP. As such, it plays an entirely different role from CSP in the analysis and characterization of chemically reacting flows.

2. Methodology

2.1. *The concept of mode separation in CSP*

In the theory of CSP, a spatially homogeneous reacting system is formulated as the following ODEs:

$$\frac{\mathrm{d}\boldsymbol{y}}{\mathrm{d}t} = \boldsymbol{g}(\boldsymbol{y}), \tag{2.1}$$

where $\boldsymbol{g}$ is the source term induced by chemical reactions, and $\boldsymbol{y}$ is the vector of the dependent variables, such as species concentrations and temperature, that are nonlinearly coupled in chemically reacting systems. Using the chain rule, (2.1) can be transformed to

$$\frac{\mathrm{d}\boldsymbol{g}}{\mathrm{d}t} = \boldsymbol{J} \cdot \boldsymbol{g}(\boldsymbol{y}), \quad \boldsymbol{J} = \frac{\partial \boldsymbol{g}}{\partial \boldsymbol{y}}, \tag{2.2}$$

where $\boldsymbol{J}$ is the Jacobian matrix of $\boldsymbol{g}$. The variables in (2.2) can then be grouped using a change of basis:

$$\frac{\mathrm{d}\boldsymbol{f}}{\mathrm{d}t} = \boldsymbol{\Lambda} \cdot \boldsymbol{f},$$
$$\boldsymbol{f} = \boldsymbol{B} \cdot \boldsymbol{g},$$

and

$$\boldsymbol{\Lambda} = \left(\frac{\mathrm{d}\boldsymbol{B}}{\mathrm{d}t} + \boldsymbol{B} \cdot \boldsymbol{J} \right) \cdot \boldsymbol{A}, \quad \boldsymbol{A} = \boldsymbol{B}^{-1}, \tag{2.3}$$

where $\boldsymbol{f}$ is the vector of modes, and matrices $\boldsymbol{A}$ and $\boldsymbol{B}$ are composed of column and row basis vectors, respectively. Ideally, a diagonal $\boldsymbol{\Lambda}$ can be obtained from (2.3) such that each mode is completely decoupled from the others. However, $\boldsymbol{J}$, and consequently $\boldsymbol{A}$ and $\boldsymbol{B}$, are time-dependent in nonlinear systems such that the ideal basis vectors are not available in general. In such cases, CSP provides a refinement procedure (Lam 1993; Lam & Goussis 1994) to obtain a pair of $\boldsymbol{A}$ and $\boldsymbol{B}$ iteratively such that $\boldsymbol{\Lambda}$ is approximately block-diagonal. The fast and slow subspaces are thereby decoupled:

$$\left.\begin{aligned}
& \frac{\mathrm{d}\boldsymbol{f}_{fast}}{\mathrm{d}t} = \boldsymbol{\Lambda}_{fast} \boldsymbol{f}_{fast}, \quad \frac{\mathrm{d}\boldsymbol{f}_{slow}}{\mathrm{d}t} = \boldsymbol{\Lambda}_{slow} \boldsymbol{f}_{slow}, \\
& \boldsymbol{\Lambda} = \begin{pmatrix} \boldsymbol{\Lambda}_{fast} & \\ & \boldsymbol{\Lambda}_{slow} \end{pmatrix}, \quad \boldsymbol{A} = \begin{pmatrix} \boldsymbol{A}_{fast} & \boldsymbol{A}_{slow} \end{pmatrix}, \quad \boldsymbol{B} = \begin{pmatrix} \boldsymbol{B}_{fast} \\ \boldsymbol{B}_{slow} \end{pmatrix}, \\
& \boldsymbol{\Lambda}_{fast} = \left(\frac{\mathrm{d}\boldsymbol{B}_{fast}}{\mathrm{d}t} + \boldsymbol{B}_{fast} \cdot \boldsymbol{J} \right) \cdot \boldsymbol{A}_{fast}, \quad \boldsymbol{\Lambda}_{slow} = \left(\frac{\mathrm{d}\boldsymbol{B}_{slow}}{\mathrm{d}t} + \boldsymbol{B}_{slow} \cdot \boldsymbol{J} \right) \cdot \boldsymbol{A}_{slow}.
\end{aligned}\right\} \tag{2.4}$$

The CSP refinement ensures that the eigenvalues of $\boldsymbol{\Lambda}_{fast}$ are all negative and have much larger magnitudes than those of $\boldsymbol{\Lambda}_{slow}$, such that the fast modes are exhausted after a transient period, i.e.

$$\boldsymbol{f}_{fast} = 0. \tag{2.5}$$

For diffusive systems, the analysis is more involved due to the interaction between transport and chemistry (Lam 1992; Goussis 1996; Hadjinicolaou & Goussis 1998; Bongers, Van Oijen & De Goey 2002; Singh, Powers & Paolucci 2002; Davis 2006; Lam 2007; Davis & Tomlin 2008). To elaborate on this point, after discretization, the conservation equations of a diffusive flow in the Eulerian coordinate system can be expressed as

$$\frac{\mathrm{D}\boldsymbol{y}}{\mathrm{D}t} = \boldsymbol{g}(\boldsymbol{y}) = \boldsymbol{\omega}(\boldsymbol{y}) + \boldsymbol{s}(\boldsymbol{y}), \tag{2.6a}$$

where $\mathrm{D}/\mathrm{D}t$ is the material derivative, $\boldsymbol{\omega}$ is the chemical source term and $\boldsymbol{s}$ is diffusion and other applicable non-chemical source terms. Note that the vector of dependent variables $\boldsymbol{y}$ includes the variables on all of the grid points. In Lagrangian coordinates, (2.6a) becomes:

$$\frac{\mathrm{d}\boldsymbol{y}}{\mathrm{d}t} = \boldsymbol{g}(\boldsymbol{y}) = \boldsymbol{\omega}(\boldsymbol{y}) + \boldsymbol{s}(\boldsymbol{y}), \tag{2.6b}$$

and $\boldsymbol{y}$ includes the spatial locations in addition to other dependent variables, such as species concentrations, velocity and the thermodynamic states, of the tracked fluid particles. In (2.6), the Jacobian matrix of the chemical source term is block-diagonal because chemical reaction is local in nature. Nevertheless, the Jacobian of the diffusion term is typically a banded matrix that couples the variables on all of the grid points. There are two different approaches to the application of CSP on a diffusive system given by (2.6). The first approach is to directly apply the refinement procedures for homogeneous systems (Lam 1993; Lam & Goussis 1994) on (2.6b), which are ODEs. This approach can be readily applied to zero- and one-dimensional systems, while it is computationally infeasible for most two-dimensional and three-dimensional systems due to the large size of the Jacobian matrix. In all likelihood, this is the primary reason why this approach has not been adopted in previous CSP studies of diffusive systems. A more efficient approach is to treat (2.6a) as partial differential equations (PDEs) and to perform the CSP refinement on individual grid points, while adding the local diffusion term to the revised formulae for the refinement (Lam 1992, 2007). If the convective term is moved to the right-hand side in (2.6a), the revised CSP refinement needs to account for convection as well (Goussis 1996; Hadjinicolaou & Goussis 1998). With either approach, the fast and slow subspaces can be decoupled with the refinement.

Once the fast modes are obtained, the species involving the fast subspace can subsequently be identified using radical pointers, defined as

$$\boldsymbol{Q} = \mathrm{diag}(\boldsymbol{A}_{fast}\boldsymbol{B}_{fast}), \tag{2.7}$$

where Q_i is normalized and indicates the degree of parallelism between the ith variable, which can be either a species or temperature, and the fast subspace. A variable is a CSP radical if the associated radical pointer is not negligible, and CSP radicals are the candidates that can be solved by the algebraic equations in (2.5) (Lam 1993; Lam & Goussis 1994). Note that although radical pointers are normalized, they can be negative or larger than unity. Therefore, special care is needed to compare radical pointers with threshold values.

Practically, the time dependence of matrix $\boldsymbol{B}$ is difficult to compute in (2.3), and has been neglected in many cases when the leading order accuracy is adequate. In such cases, (2.3) can be replaced by a simple eigendecomposition (Maas & Pope 1992; Lu *et al.* 2001; Kazakov *et al.* 2006), i.e.

$$\boldsymbol{\Lambda} = \boldsymbol{B} \cdot \boldsymbol{J} \cdot \boldsymbol{A}, \quad \boldsymbol{A} = \boldsymbol{B}^{-1}, \tag{2.8}$$

and $\boldsymbol{\Lambda}$ is diagonal if $\boldsymbol{J}$ is not defective such that the modes are fully decoupled with leading order accuracy. Complex eigenvalues of $\boldsymbol{J}$ indicate the existence of oscillatory modes (Lu *et al.* 2001), the significance of which has been investigated for the ignition of large hydrocarbons (Kazakov *et al.* 2006).

The study of explosive modes with CSP, however, has thus far been only preliminary, and it has not been applied to the analysis of turbulent reactive flows. In the following sections, the concepts of mode separation and radical pointer from CSP will be adopted to develop the method of CEMA for the characterization of spatially homogeneous as well as diffusive flows and subsequently be applied to detect flame and ignition fronts in chemically reacting flows.

2.2. *Quantification of chemical explosive modes*

Chemical explosive modes are associated with positive eigenvalues, λ_{exp}, of the Jacobian, $\boldsymbol{J}_{\omega}$, of the chemical source term, $\boldsymbol{\omega}$, in (2.6), i.e.

$$\mathrm{Re}(\lambda_{exp}) > 0. \tag{2.9}$$

A complex λ_{exp} frequently indicates an oscillatory chemical mode, with the real part of λ_{exp} corresponding to the reciprocal time scale of the explosion, and the imaginary part indicating the oscillation frequency. In the present study, we will focus only on the real part of λ_{exp}.

Once the chemical explosive mode is identified, a concept similar to the radical pointer can be defined:

$$\boldsymbol{EP} = \mathrm{diag}(\boldsymbol{a}_{exp}\boldsymbol{b}_{exp}), \tag{2.10}$$

where $\boldsymbol{a}_{exp}$ and $\boldsymbol{b}_{exp}$ are the right and left eigenvectors, respectively, associated with a λ_{exp} of $\boldsymbol{J}_{\omega}$. Similarly, $\boldsymbol{EP}$ is dimensionless and its ith entry, EP_i, indicates the degree of parallelism between the ith variable and the explosive mode. To avoid confusion with the radical pointer, $\boldsymbol{EP}$ will be referred to as the 'explosion pointer' in the following.

It is important to recognize that the chemical explosive mode, so defined, is mathematically distinctive from the CSP mode, in that the chemical explosive mode is strictly a chemical property. Therefore, it can interact with non-chemical processes, such as diffusion, and other non-explosive chemical modes. On the other hand, the CSP modes in homogeneous systems are decoupled and evolve independently if $\boldsymbol{\Lambda}$ in (2.4) is diagonal. In diffusive systems, a refined CSP mode depends on both chemistry and diffusion (Lam 1992; Goussis 1996; Lam 2007), and hence, it is not a chemical property. Thus the properties and restrictions of CSP modes do not necessarily apply to the chemical explosive modes. Under special circumstances, for example, when chemistry dominates over diffusion and the chemical Jacobian is primarily time-independent, a chemical explosive mode may indeed also be a CSP mode. In the following discussion, a mixture is defined to be explosive if a chemical explosive mode exists, recognizing nevertheless that an explosive mixture does not always results in explosion or ignition, for example in a strained flow.

The existence of chemical explosive modes and the concept of the explosion pointer are demonstrated in figure 1 for the auto-ignition of a homogeneous, stoichiometric hydrogen–air mixture. The detailed hydrogen–air kinetic mechanism used is from
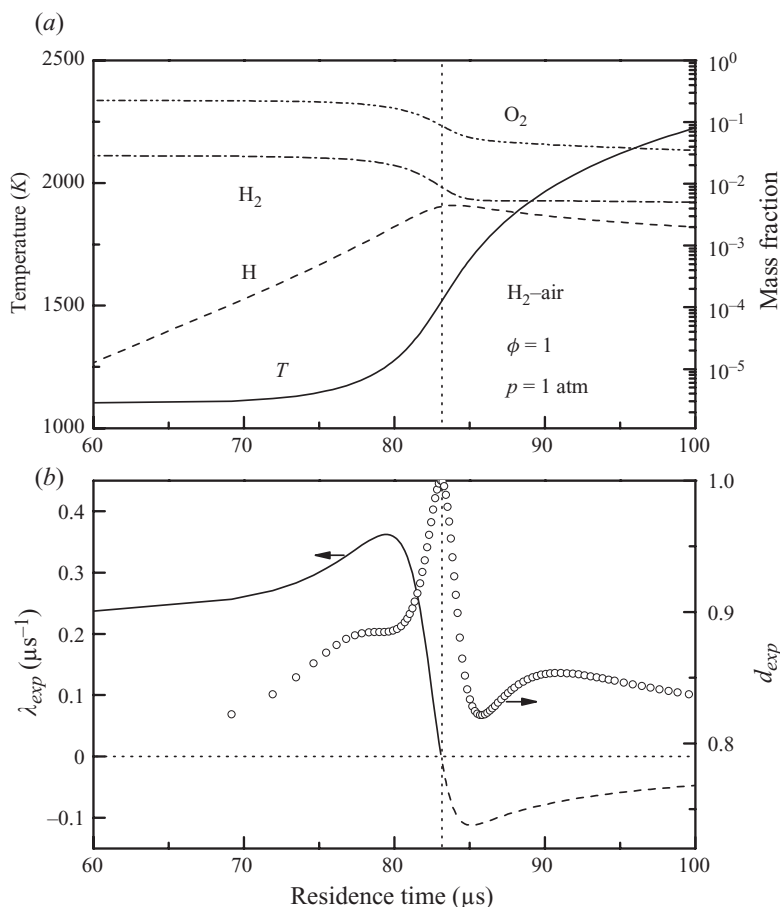
FIGURE 1. Temperature and selected species profiles in auto-ignition of a stoichiometric hydrogen–air mixture under atmospheric pressure and an initial temperature of 1100 K. (*a*) Temperature and species concentrations and (*b*) time scale, λ_{exp}, of the explosive mode and the defectiveness index, d_{exp}, of the chemical Jacobian. The dotted lines indicate the crossover point, where $\lambda_{exp} = 0$.

Li *et al.* (2004). Figure 1(*a*) shows the temperature and mass fractions of selected species, namely H, H_2 and O_2, and figure 1(*b*) shows the time scale of the chemical explosive mode. It is seen that the mixture is explosive before ignition, as indicated by a positive λ_{exp}, and is non-explosive after ignition since λ_{exp} becomes negative. Henceforth, the state at which λ_{exp} crosses zero is referred to as the 'crossover point'. For auto-ignition, where transport is absent, the crossover point typically corresponds to the inflection point in the temperature profile in figure 1(*a*), which is a widely accepted definition of the ignition point. For additional information of the post-ignition mixtures, a negative λ_{exp} in figure 1(*b*) is the eigenvalue of the slowest decaying mode, which was evolved from the chemical explosive mode in the pre-ignition mixtures.

   Figure 2(*a*) shows the explosion pointers for temperature and selected species. An interesting observation is that the explosion pointers diverge as they approach the crossover point, indicating the existence of a singularity. A similar trend was also observed for hydrocarbons. This singularity can be explained by noting from
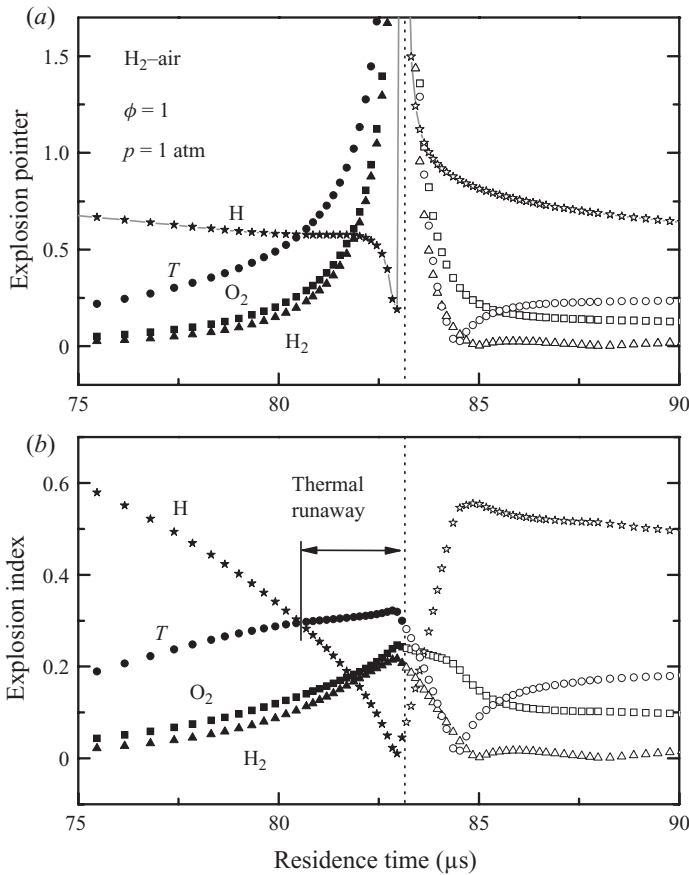
FIGURE 2. (*a*) Explosion pointers and (*b*) explosion indices for temperature and selected species in auto-ignition of a stoichiometric hydrogen–air mixture under atmospheric pressure and an initial temperature of 1100 K. The dotted lines indicate the crossover point, where $\lambda_{exp} = 0$.

figure 2(*a*) that while the explosion pointer for temperature becomes more positive near the singularity, that of the reactants, i.e. H_2 and O_2, becomes more negative indicating that the effect of thermal runaway is balanced by the consumption of reactants at the crossover point. A closer inspection of the eigenvector of the explosive mode shows that the explosive mode rotates into the subspace of the energy and element conservation modes through thermal runaway, such that the Jacobian lacks a complete set of eigenvectors, that is being defective, at the crossover point. To demonstrate this point, a defectiveness index, d_{exp}, is defined for the chemical explosive mode:

$$d_{exp} \equiv \boldsymbol{b}_e \cdot \boldsymbol{b}_a, \ \boldsymbol{b}_a = \boldsymbol{b}_e \boldsymbol{B}_c^{\mathrm{T}} \left(\boldsymbol{B}_c \boldsymbol{B}_c^{\mathrm{T}} \right)^{-1} \boldsymbol{B}_c, \quad (2.11)$$

where $\boldsymbol{b}_e$ is $\boldsymbol{b}_{exp}$ normalized to unit length. Each row of matrix $\boldsymbol{B}_c$ is a left eigenvector for the element or energy conservation mode. Note that $\boldsymbol{b}_a$ is the best approximation of $\boldsymbol{b}_e$ that can be spanned by the conservation modes. Therefore, d_{exp} being unity, as shown in figure 1(*b*) at the crossover point, indicates that the chemical explosive mode is completely spanned by the conservation modes, such that the Jacobian matrix is defective. Consequently, although the entries in $\boldsymbol{EP}$ sum to unity, each explosion pointer can be arbitrarily large near the singularity. This renders it difficult to use

the explosion pointers near ignition. To resolve this difficulty, the explosion pointers defined in (2.10) are normalized as

$$EI = \frac{\mathrm{abs}(\boldsymbol{EP})}{\mathrm{sum}(\mathrm{abs}(\boldsymbol{EP}))}, \qquad (2.12)$$

where $\boldsymbol{EI}$ is henceforth referred to as the 'explosion index' for distinction. Note that, although the explosion indices are normalized to [0, 1] in (2.12), they should not be evaluated too close to the singularity because of the growing numerical error in obtaining the inverse of the ill-conditioned matrix $\boldsymbol{A}$ there.

Figure 2(b) shows the explosion index for temperature and species which participate non-trivially in the explosive mode for the auto-ignition in figure 1. It is seen that the explosion indices evolve continuously across the ignition point despite the existence of the singularity, and as such, the explosion index at the crossover point may be obtained through extrapolation, if needed. It is further seen that there are two stages in the ignition process, namely radical explosion and thermal runaway, separated by the point where the explosion index profile for temperature crosses that of the H radical, at approximately 80.4 µs in residence time. The radical explosion stage is manifested by the exponential growth in the H radical in a nearly isothermal environment, as shown by the linear segment of the H profile in figure 1(a). In figure 1(b), it is observed that the time scale of the explosive mode changes only slightly during radical explosion. Thermal runaway occurs near the end of the ignition process, where the temperature varies dramatically and the explosion index of radical H becomes small in figure 2(b).

Since the chemical explosive mode is a chemical property of the mixture, its time scale and the associated explosion indices can be utilized to distinguish between unburnt and burnt mixtures. Specifically, if a chemical explosive mode exists in a reactive mixture, the mixture will eventually explode if it is isolated in an adiabatic and unstrained environment. In such cases, the mixture can be classified as unburnt. The mixture can be classified as burnt otherwise. Figure 3 demonstrates the structure of the chemical explosive mode in a one-dimensional freely propagating laminar premixed flame. Note that the chemical explosive mode only exists in the preheat zone where the mixture is unburnt. It is seen that the time scale for the explosive mode first increases as temperature rises, and then crosses over to negative values when the mixture is burnt. Similar to figure 1(b), the transition from an explosive to a non-explosive mixture occurs near the end of thermal runaway, such that it forms an abrupt zone that is even thinner than the reaction zone and sharply demarcates the burnt and unburnt mixtures. To further verify the validity of this measure over a wide range of mixtures, the temperature profiles of lean to rich premixed H_2–air flames are plotted in figure 4, with the time scales of the explosive modes superimposed in colour. Note that the transition from explosive to non-explosive mixture is abrupt, compared with the flame thickness, for each of the five cases, while the change within the unburnt zone is smooth. Therefore the sharp boundary is a useful property of many premixed flames and can be utilized to detect premixed or partially premixed flame fronts in complex flow fields.

Figure 3(b) plots the explosion indices for temperature and species, and shows that, contrary to the homogeneous ignition in figures 1 and 2, no radical explosion is observed for the flame. In particular, the explosion index for temperature dominates in the entire preheat zone, although the H radical still participates in the explosion to a moderate extent. This is because the strong back diffusion of the H radical from the burnt mixture dominates over the local generation of H through chemical branching
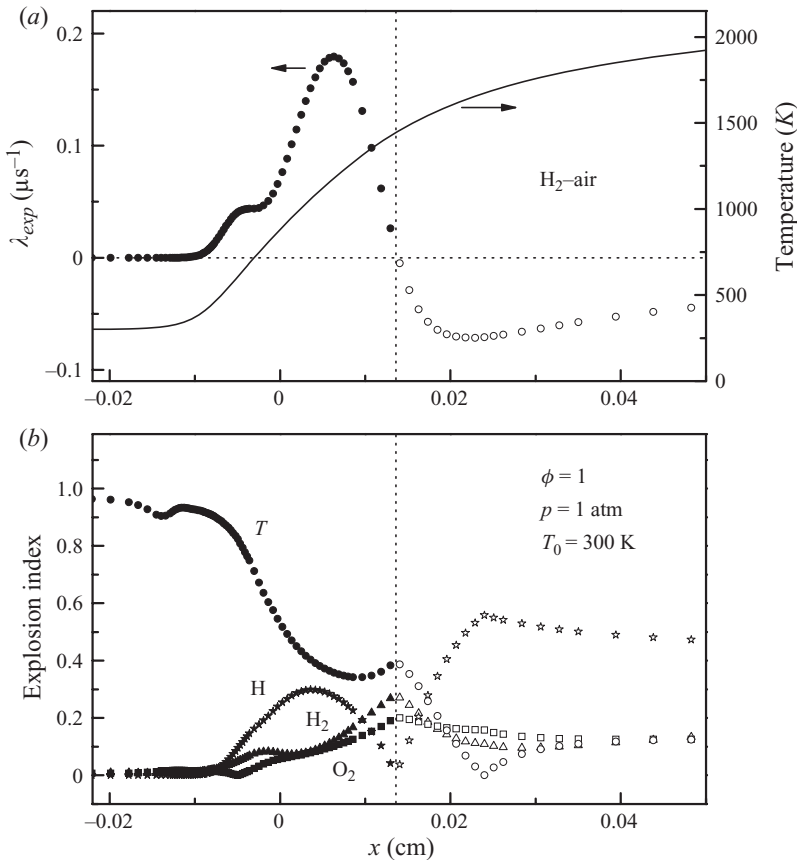
FIGURE 3. Explosive mode in a one-dimensional freely propagating laminar premixed flame with a stoichiometric hydrogen–air mixture at STP. (*a*) Time scale of the explosive mode and temperature (*b*) explosion indices of temperature, H, H_2 and O_2. The dotted lines indicate the crossover point where $\lambda_{exp} = 0$.

in the preheat zone, such that radical explosion is not important in building up the radical pool in thepreheat zone. This distinguishing feature can be used to detect whether a reaction front is dominated by flame propagation or auto-ignition.

We now extend these observations in homogeneous and diffusive systems to analyse the region near the flame base of a turbulent lifted jet flame described in Yoo *et al.* (2009).

3. Results and discussion

3.1. *Configuration and selected results of the DNS*

A description of the detailed configuration of the DNS can be found in Yoo *et al.* (2009). To summarize, three-dimensional DNS of a turbulent lifted hydrogen jet flame in a heated coflow was performed using the Sandia DNS code, S3D (Chen *et al.* 2009). This code solves the compressible Navier–Stokes equations with a fourth-order explicit Runge–Kutta method for time integration, and an eighth-order centred finite difference scheme for spatial differentiation. The detailed kinetic mechanism used in the DNS is from Li *et al.* (2004). The inlet fuel jet consists of 65 % hydrogen and
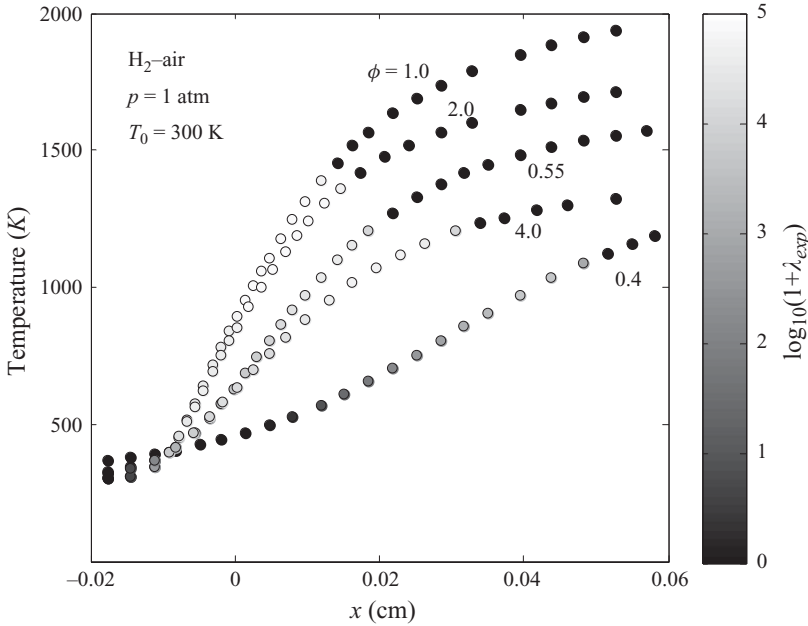
FIGURE 4. Temperature profiles of hydrogen–air mixtures for different equivalence ratios, coloured with the time scales of the explosive modes. Negative eigenvalues are truncated to zero.

35 % nitrogen by volume under atmospheric pressure, at a temperature of 400 K, and with a jet velocity of $347\,\mathrm{m\,s^{-1}}$. The coflowing air is at 1100 K and has a velocity of $4\,\mathrm{m\,s^{-1}}$. The jet Reynolds number is 11 000 based on the width of the slot, H, which is 1.92 mm. The size of the computational domain is 24 mm by 32 mm by 6.4 mm in the streamwise (x), transverse (y) and spanwise (z) directions, respectively, and 944 million grid points were required to resolve both the Kolmogorov length scale and the flame/ignition structure. Non-reflecting inflow/outflow boundary conditions are imposed in the streamwise and transverse directions, and periodic boundary conditions are imposed in the spanwise direction. A flow-through time, $\tau_j (\equiv L_x/U_j)$, based on the inlet jet velocity (U_j) and the streamwise domain length (L_x), is approximately 0.07 ms. The flow field was artificially ignited at $t = 0$ and was integrated at a constant time step of 4 ns until the flame became statistically stationary, through $8\tau_j$. Subsequently, the simulation was integrated for four more flow-through times to provide converged statistics for model validation and development. The simulation was performed on a Cray XT3/XT4 at Oak Ridge National Laboratories and used approximately 3.5 million CPU-hours on 10 000 processors. A representative two-dimensional spanwise slice at $t/\tau_j = 12$ and $z = 0$ was selected from the 30 terabytes of raw data for the following analysis.

   Figure 5 shows spatial profiles of selected results from the simulation. Figure 5(a–c) shows the structure of the flow field in terms of temperature, mixture fraction based on Bilger's definition (Bilger 1988) and heat release rate. Figure 5(d–f) shows the concentrations of three important radicals. This information facilitates the understanding of the structure of the lifted flame. Specifically, figure 5(a) shows three bulk regions: unburnt cold fuel near the jet centre (dark), preheated air (grey) and the burnt mixtures in the mixing layer (light). Therefore, the position where the flame is stabilized can approximately be identified as the leading edge of the high
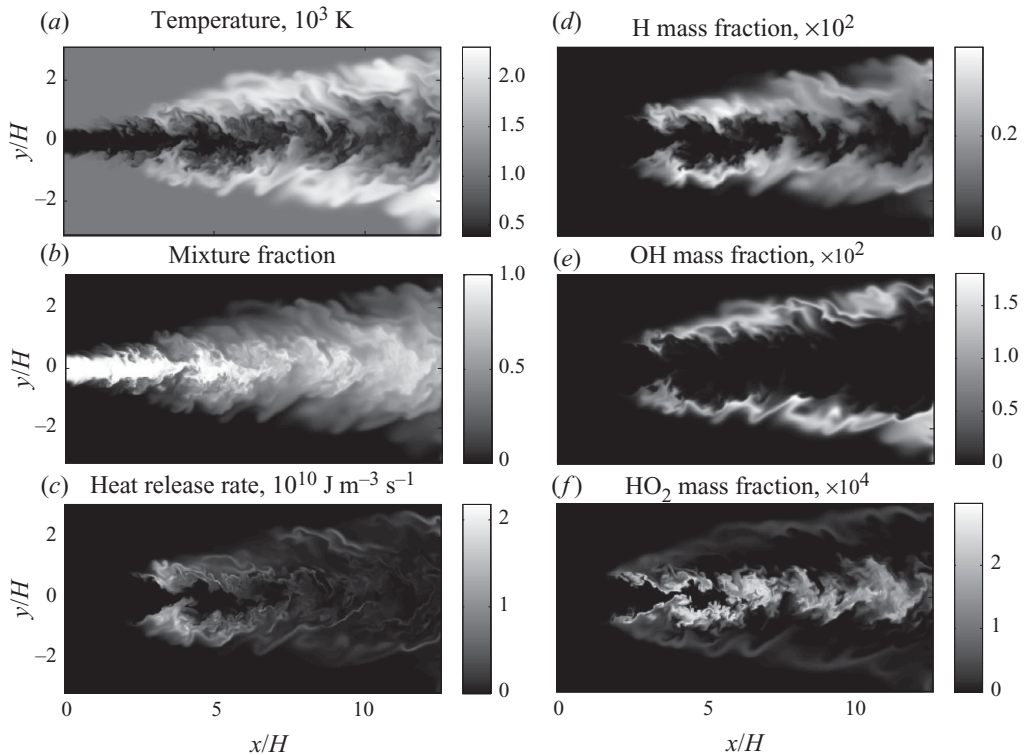
FIGURE 5. The spatial distribution of temperature, mixture fraction, heat release rate and species mass fractions from a spanwise slice from DNS of a H_2 jet issuing into preheated air at $t/\tau_j = 12$ and $z = 0$ (Yoo *et al.* 2009).

temperature zone. Figure 5(b) shows the structure of the mixing layer. It demonstrates, not surprisingly, that high temperature is observed in well-mixed regions, and the highest temperature is correlated with slightly rich mixtures with mixture fractions between 0.2 and 0.3, where the stoichiometric mixture fraction is $\xi_{st} = 0.199$. The heat release rate attains its maximum value primarily near the leading edge of the mixing layer where the temperature is high. Due to the Arrhenius effect, the reaction rate is very sensitive to temperature fluctuations. Furthermore, fast reactions typically are not self-sustainable due to the rapid depletion of reactants, such that large reaction rates are typically transient, resulting in the presence of distributed small hotspots and thin layers present in the heat release rate plot.

Figure 5(d–f) shows the profiles for H, OH and HO_2, respectively. Since H is a crucial radical for hydrogen and hydrocarbon fuels, and high concentration of H typically indicates strong chemical reactions that are sensitive to temperature, a clear correlation between H concentration and temperature is observed. Next, we note that since OH is an important experimental flame marker, and is a fairly good QSS species (Lu, Law & Ju 2003), its concentration strongly depends on both temperature and H concentration. Moreover, H and OH typically peak in the reaction zone of flames and slowly diminish in the recombination zone where temperature approaches the adiabatic value. Therefore, regions with high concentrations of H and OH approximately coincide with regions of high temperature, with the exception of a slight offset in their maximum positions. Nevertheless, in contrast to H and OH,
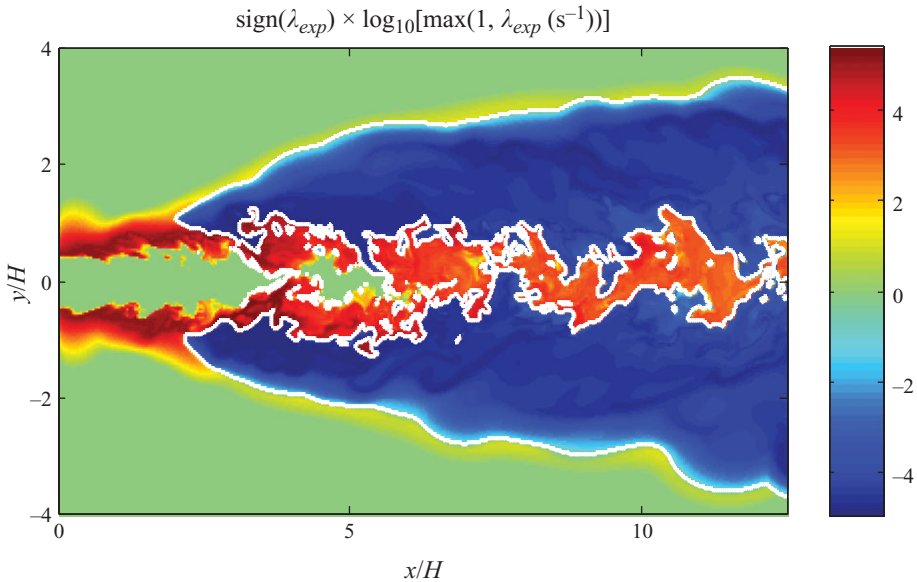
$$\text{sign}(\lambda_{exp}) \times \log_{10}[\max(1, \lambda_{exp}\ (\text{s}^{-1}))]$$

FIGURE 6. Spatial distribution of the time scale of local chemical explosive modes from a spanwise slice from DNS of a H_2 jet issuing into preheated air at $t/\tau_j = 12$ and $z = 0$ (Yoo *et al.* 2009). A negative value of λ_{exp} is the eigenvalue associated with the slowest decaying mode in a non-explosive mixture. The boundary between non-explosive and explosive regions is delineated by a white isocontour at $\lambda_{exp} = 0$.

HO_2 typically peaks in igniting mixtures in the fuel-lean preheat zone or in ignited mixtures near the fuel-rich reaction zones of flames and is depleted in the post flame zones, as shown in figure 5.

While the scalar fields shown in figure 5 are very illuminating in terms of the basic structure of the lifted flame, there is insufficient information to accurately pinpoint the location of the flame fronts and the stabilization point in the flow field. This is because flame fronts are typically very thin, whereas there is no clearly visible sharp boundary in any of the profiles in figure 5. Furthermore, most of the quantities shown are severely affected by the local equivalence ratio, which spans the entire range of conditions from extremely lean to extremely rich across the mixing layer. As such, the exact locations of the flame fronts may be difficult to discern from plots of conventional scalars, for example those shown in figure 5, especially if the flame is located, for example, in an extremely lean region.

In light of these constraints, CEMA is applied to detect the presence of flames, particularly the lean premixed fronts, and thereby attain further understanding of the stabilization mechanism of lifted hydrogen flames in a heated coflow.

3.2. *CEMA for the lifted flame*

The method of CEMA was performed at each grid point in the flow field shown in figure 5. The eigenvalue, or the reciprocal time scale, of the chemical explosive mode is presented in figure 6. Note that modes with time scales longer than 1 s are considered dormant compared with the flow-through time of 0.07 ms, and hence, are truncated to 1 s to simplify the visualization. The least-negative eigenvalue aside from the zero eigenvalues associated with the conservation modes is displayed for non-explosive mixtures in figure 6. Non-explosive regions are denoted by blue, while

explosive regions are denoted by warmer colours. The pair of non-explosive zones corresponding to the two halves of the jet are separated from explosive mixtures by a white isocontour at $\lambda_{exp} = 0$, from the fork-shaped explosive mixtures. Note that the transition between the explosive and non-explosive mixtures is abrupt compared with the size of the local flow structure, particularly on the air side. Such a sharp transition in chemical explosivity is attributed to the existence of a thin chemical reaction zone in the present flame, similar to the laminar premixed flame in figure 3. The white isocontour therefore delineates the flame fronts, which enclose non-explosive regions with burnt mixture as roughly indicated in the temperature plot of figure 5. The explosive regions therefore are composed of unburnt mixture into which the flame propagates. The bifurcation point of the fork preceding the lean and the rich flame fronts corresponds to the location where the first parcel of burnt mixture appears, and as such, it unambiguously defines the stabilization point of the lifted flame.

It is further observed that there are two major segments of flame fronts, one near the central fuel-rich jet and the other in the fuel-lean heated air coflow. The rich flame front is severely corrugated due to intense turbulence in the cold central jet, while the lean flame front is nearly laminar as it exists in a hot, low velocity coflow. While the rich flame fronts delineated by the CEMA are similar to those delineated by high HO_2 concentrations shown in figure 5, the lean flame fronts are only visible from the explosive mode plot since the mixture is extremely lean, with a local equivalence ratio less than 0.01, such that the temperature increase across the flame is basically indiscernible and both fuel and radical concentrations are extremely low. The explosivity of the mixture diminishes further into the coflowing air due to the vanishing fuel concentration. Another barely explosive region can be observed near the jet centre immediately downstream of the jet inlet, where oxidizer is essentially absent.

It is clear that the mixture in the mixing layer upstream of the stabilization point is highly explosive, as indicated by the dark-red colours in figure 6. The time scale of the explosive mixture is comparable to the flow transit time from the jet inlet to the stabilization point, suggesting that auto-ignition, rather than flame propagation, is the controlling factor determining the lift-off height. To further verify this point, a Damköhler number is defined as

$$Da = \lambda_{exp} \cdot \chi^{-1}, \tag{3.1}$$

where χ is the local instantaneous scalar dissipation rate, defined as $\chi = 2\alpha|\nabla\xi|^2$, where ξ and α are mixture fraction and thermal diffusivity, respectively. The Damköhler number, so defined, indicates how fast the explosive mode is compared with transport. If $Da \gg 1$, the chemical explosive mode is much faster than mixing and will lead to ignition. Otherwise, the chemical explosive mode may be inhibited by excessive mixing rates and ignition may not progress to thermal explosion. The Da structure plotted in figure 7 is similar to the eigenvalue plot in figure 6 and clearly shows two thin wrinkled layers of auto-igniting mixtures with $Da \gg 1$ (in dark red), each of which culminates at the stabilization point. Therefore, the stabilization mechanism is unambiguously attributed to auto-ignition.

Finally, to demonstrate that the stabilization point is not significantly affected by flame propagation, the explosion index, defined in (2.12), is presented in figure 8 for H radical and temperature, respectively. As discussed earlier in the context of premixed flame structure in figure 3, radical explosion is not important in the preheat zone of a flame, while it is a necessary precursor to the accumulation of a radical pool for auto-ignition. Therefore, a typical premixed flame front is preceded by a rather
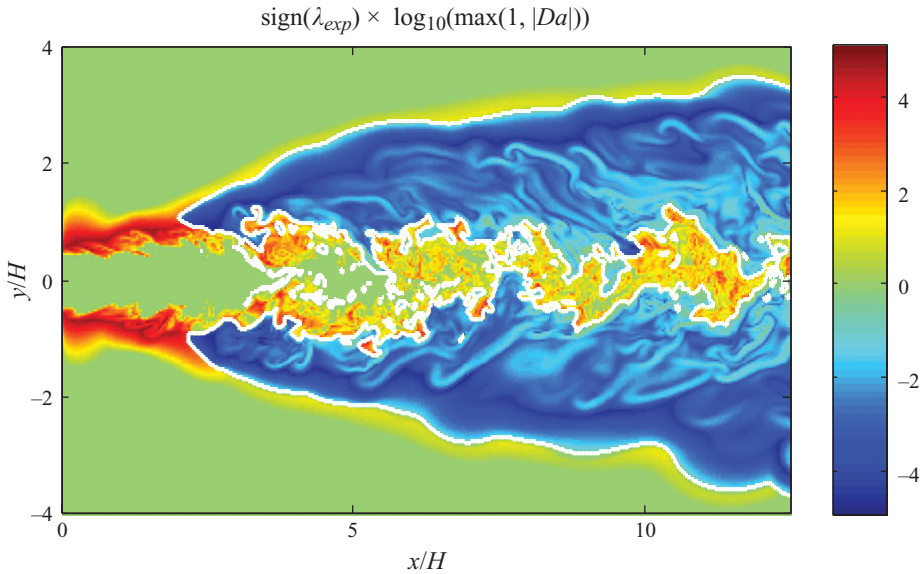
$$\text{sign}(\lambda_{exp}) \times \log_{10}(\max(1, |Da|))$$

FIGURE 7. Spatial distribution of the Damköhler number from DNS of a H_2 jet issuing into preheated air at $t/\tau_j = 12$ and $z = 0$ (Yoo *et al.* 2009), superimposed with the flame fronts identified by CEMA (white isocontour). Time scales longer than 1 s were truncated to 1 s for both the explosive mode and the scalar dissipation rate in computing *Da*.

wide thermal runaway zone as shown in figure 3, while the thermal runaway zone for auto-ignition is comparatively thinner as shown in figure 1(*b*). In figure 8, it is clearly observed that radical explosion dominates almost the entire stream of the highly explosive mixture leading to the stabilization point, whereas thermal runaway is observed only in the vicinity of the stabilization point.

In summary, the stabilization mechanism of the present lifted hydrogen flame in heated coflow is characterized by the following sequence of events in the downstream development of the jet. First, the reactants undergo mixing at the jet inlet and form a thin layer of fuel-lean mixture at near ambient temperature. This highly explosive mixing layer is then convected downstream and the radical pool builds up in a near-homogeneous environment. The explosive mixture finally ignites at the stabilization point after transient thermal runaway, resulting in the formation of the leading edge of the two premixed flames. Downstream of the stabilization point the lean flame propagates outward from the mixing layer and decelerates as it approaches the lean flammability limit where the flow is laminar, whereas the rich flame propagates toward the jet centre until it approaches the rich flammability limit. The rich flame front is severely wrinkled and is disrupted by the intense turbulence, leading to the formation of islands of burnt and unburnt mixtures. The mixture loses its chemical explosivity after it crosses the flame, forming the bulk of the non-explosive regions within which diffusion-controlled burning continues downstream. The existence of a non-premixed flame in the burnt mixtures was verified and analysed in Yoo *et al.* (2009). Further study of the non-premixed flames is beyond the scope of the present CEMA, and other methods are needed for this purpose. Note that while the present lifted flame is shown to be stabilized by auto-ignition due to the high coflow temperature upstream of the stabilization point, flame propagation may still be the dominant stabilization mechanism for lifted flames with low coflow temperatures.
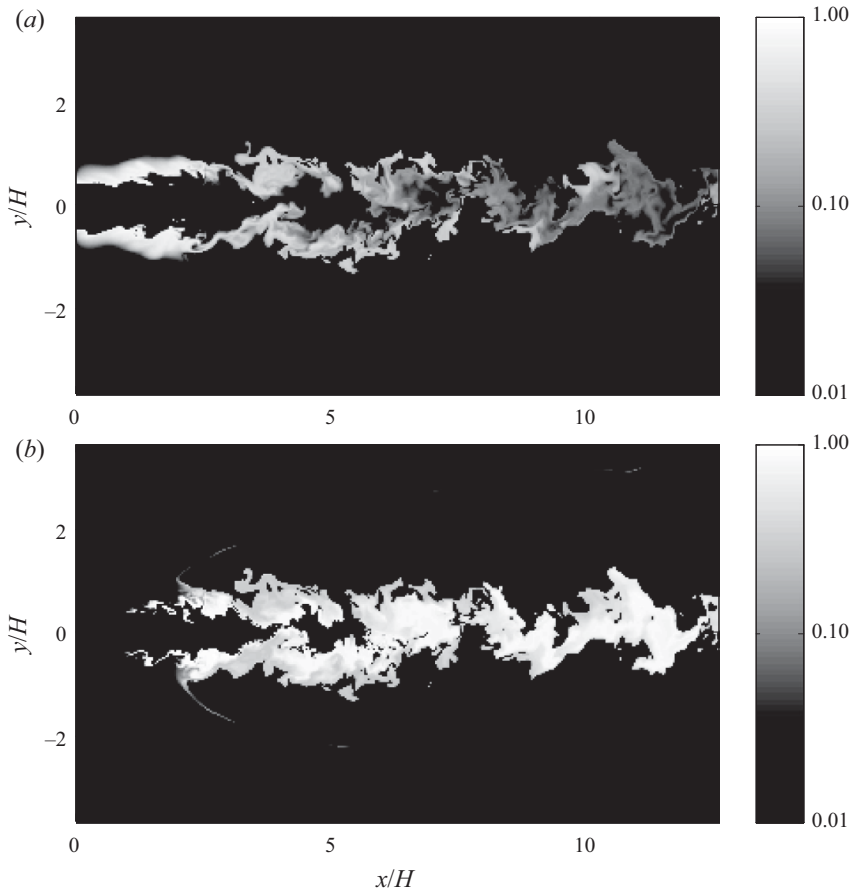
FIGURE 8. Spatial distribution of the explosion index for (*a*) H radical and
(*b*) temperature, respectively.

3.3. *Comparison with flame index and other methods*

The flame index (Yamashita *et al.* 1996) is defined as

$$FI = \nabla Y_F \cdot \nabla Y_O. \tag{3.2}$$

FI is a useful indicator to identify and distinguish premixed and non-premixed flames
in complex flows, where *F* denotes the fuel and *O* the oxidizer. In typical premixed
flames the gradients of fuel and oxidizer are aligned, such that the rapid consumption
of the reactants across the flame results in a large positive value of the flame index.
In non-premixed flames the gradients of fuel and oxidizer oppose one another, and
the flame index is negative. The magnitude of the flame index increases as the flame
becomes thinner.

The concept of the flame index differs from the present method of CEMA in two
regards. First, the chemical explosive mode is a chemical property of the mixture, while
the flame index is not. Rather, the flame index is a measure of the alignment of scalar
gradients independent of the progress of reaction. Therefore, the flame index may
also peak in non-reactive flows, such as in premixed or non-premixed opposed jets at
room temperature, and the magnitude of the flame index may be large solely due to
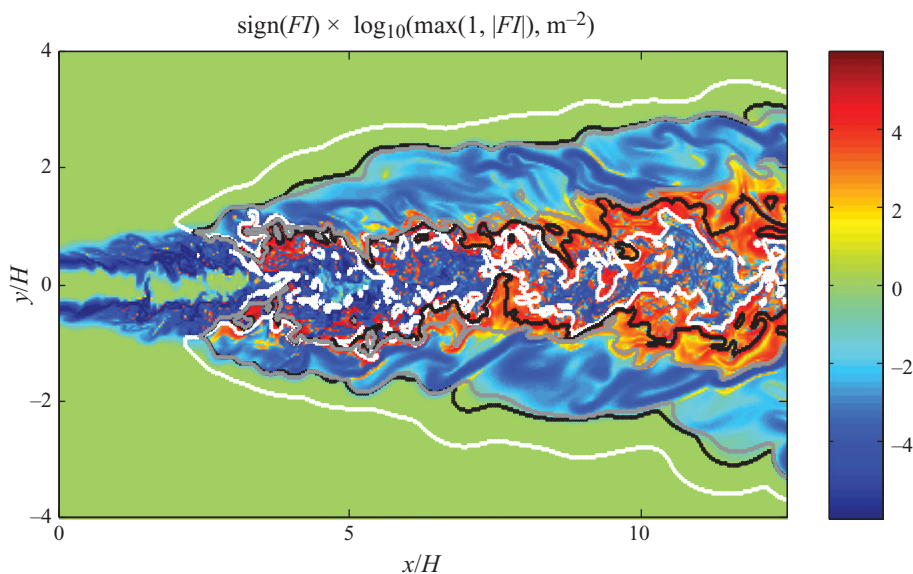high flow strain and mixing rates. Therefore, a flame may or may not actually exist

$$\text{sign}(FI) \times \log_{10}(\max(1, |FI|), \text{m}^{-2})$$

FIGURE 9. Spatial distribution of the flame index from DNS of a H_2 jet issuing into preheated air at $t/\tau_j = 12$ and $z = 0$ (Yoo *et al.* 2009), superimposed with the flame fronts identified by CEMA (white), a temperature isocontour of $T = 1150K$ (black) and an isocontour of $Y_{OH} = 0.001$ (grey).

where the flame index peaks, and an additional reaction progress variable is required to delineate the different combustion modes. Second, the flame index is subjected to similar problems as the other quantities shown in figure 5, i.e. the variation in the flame index may be difficult to discern in extremely lean mixtures, whereas ultra-lean flames can readily be discerned by CEMA. To demonstrate these points, isocontours of the flame index for the lifted flame are shown in figure 9, superimposed with various definitions of ignition/flame fronts including that from CEMA identified in figure 6, a temperature isotherm of 1150 K and $Y_{OH} = 0.001$. Note that the temperature- and OH-based definitions, adopted from Yoo *et al.* (2009), demarcate the beginning of thermal runaway, defined as 5 % of the their maximum increase in the domain. This region is located slightly downstream of the more rigorous CEMA definition. Note also that negative peaks of the flame index are observed in the mixing layer upstream of the stabilization point where no flame exists; these peaks are induced by the mixing process. Nevertheless, the combination of flame index and heat release rate analysis is a viable criterion to identify non-premixed ignition/flame fronts within the mixing layer, as reported in Yoo *et al.* (2009).

It is further seen in figure 9 that the lean flame fronts are not readily visible in the flame index plot because of the extremely low equivalence ratio there. Other methods based on isocontours of, for example, temperature and OH concentration, used in Yoo *et al.* (2009), have similar restrictions as those of the flame index as shown by the isocontours. Therefore CEMA is a unique utility for detection of weak flame fronts in extremely lean mixtures.

3.4. *Applicability of CEMA*

As mentioned in the previous section, the chemical explosive mode is defined only for the Jacobian of the chemical source term, and as such it is a chemical property of the mixture. In contrast, a CSP mode in a diffusive system depends on both

chemistry and diffusion. In the present study, while the auto-igniting mixtures can be identified in regions where a chemical explosive mode dominates diffusion, the application of CEMA to flames with strong diffusion will require further information on chemistry–flow interaction. For example, in identifying the flame fronts in the lifted hydrogen flame, the thickness of the transition zone of the chemical explosive mode is compared with the size of the local flow structure, such that the width of the thin reaction zone of the flame is implicitly employed in detecting the flame fronts. Similarly, while the present form of CEMA is not directly applicable to non-premixed flames controlled by mixing, it may be applied together with other methods, such as those based on flame index, to study complex flow fields where non-premixed flames coexist with premixed flames.

It is important to note that studying the chemical explosive mode in a diffusive system does not imply that diffusion can be neglected for a flame, or equivalently, conclusions about a flame drawn from CEMA without consideration of transport effects could be erroneous. The interaction between chemical explosive modes and diffusion in reacting flows merits further study.

Finally, it is worth mentioning that CEMA in the present work was performed with the Jacobian matrices analytically evaluated based on species molar production rates and mole concentrations. Temperature dependency of species enthalpy and heat capacity was further excluded from the chemical Jacobian for simplicity. It was found that the Jacobian matrices obtained through numerical perturbation typically do not have sufficient number of significant digits, such that the chemical explosive mode, both the eigenvalue and the associated eigenvectors, may not be accurately resolved in the presence of extremely short species time scales in the detailed mechanism.

4. Conclusions

Chemical explosive modes in chemically reacting flows were studied based on the concept of CSP and presented as a new diagnostic tool delineating ignition and flame fronts in complex flows. An abrupt change in the mixture explosivity was employed for the detection of premixed flame fronts, which are difficult to detect using conventional methods involving only individual parameters such as temperature, mixture fraction, heat release rate and species concentrations.

A singular eigenvector matrix, or defective chemical Jacobian, was observed at the crossover point of the chemical explosive mode. It was found that the singularity was caused by the convergence of the explosive mode to the conservation modes. A species explosion index was consequently defined to normalize the diverging explosion pointers near the singularity. Radical explosion and thermal runaway were then distinguished with the explosion pointers for auto-ignition. The present method was first tested on homogeneous auto-ignition and one-dimensional laminar premixed flames and subsequently applied to analyse the DNS results of a turbulent lifted hydrogen jet flame in a heated coflow. Lean laminar and rich turbulent flame fronts were detected, and the bifurcation point preceding the two flame fronts was identified as the stabilization point. A Damköhler number based on the time scale of the explosive mode and the scalar dissipation rate was defined to identify auto-igniting mixtures, and the role of auto-ignition as the mechanism for stabilization of the lifted flame was discussed.

It is important to note that the present results are relevant only to the stabilization in heated coflows in which the mixing layer formed is sufficiently hot to induce

auto-ignition. When the coflow is cold, as in the case of ambient air, stabilization may be attributed to other effects such as flame propagation against a diverging flow.

In addition to lifted flames, explosive chemical modes can also provide useful information in other flows, such as those involving the unsteady flame propagation through auto-igniting mixtures, and turbulence-induced local extinction and re-ignition. Chemical explosive modes are also important in the study of the turning points on extinction and ignition curves for steady-state flows. Such topics are interesting extensions of the present work.

REFERENCES

BILGER, R. W. 1988 The structure of turbulent nonpremixed flames. *Proc. Combust. Inst.* **22**, 475–488.

BONGERS, H., VAN OIJEN, J. A. & DE GOEY, L. P. H. 2002 Intrinsic low-dimensional manifold method extended with diffusion. *Proc. Combust. Inst.* **29**, 1371–1378.

CABRA, R., MYHRVOLD, T., CHEN, J. Y., DIBBLE, R. W., KARPETIS, A. N. & BARLOW, R. S. 2002 Simultaneous laser Raman-Rayleigh-LIF measurements and numerical modelling results of a lifted turbulent H2/N2 jet flame in a vitiated coflow. *Proc. Combust. Inst.* **29**, 1881–1888.

CHEN, J. H., CHOUDHARY, A., DE SUPINSKI, B., DEVRIES, M., HAWKES, E. R., LASKY, S., LIAO, W. K., MA, K. L., MELLOR-CRUMMEY, J., PODHORSZKI, N., SANKARAN, R., SHENDE, S. & YOO, C. S. 2009 Terascale direct numerical simulations of turbulent combustion using S3D. *Comput. Sci. Disc.* **2**, 015001.

CHUNG, S. H. 2007 Stabilization, propagation and instability of tribrachial triple flames. *Proc. Combust. Inst.* **31**, 877–892.

DAVIS, M. J. 2006 Low-dimensional manifolds in reaction–diffusion equations. Part I. Fundamental aspects. *J. Phys. Chem.* A **110**, 5235–5256.

DAVIS, M. J. & TOMLIN, A. S. 2008 Spatial dynamics of steady flames. Part I. Phase space structure and the dynamics of individual trajectories. *J. Phys. Chem.* A **112**, 7768–7783.

FOTACHE, C. G., KREUTZ, T. G. & LAW, C. K. 1997 Ignition of counterflowing methane versus heated air under reduced and elevated pressures. *Combust. Flame* **108**, 442–470.

GORDON, R. L., MASRI, A. R., POPE, S. B. & GOLDIN, G. M. 2007 A numerical study of auto-ignition in turbulent lifted flames issuing into a vitiated co-flow. *Combust. Theory Model.* **11**, 351–376.

GOUSSIS, D. A. 1996 On the construction and use of reduced chemical kinetic mechanisms produced on the basis of given algebraic relations. *J. Comput. Phys.* **128**, 261–273.

GOUSSIS, D. A. & NAJM, H. N. 2006 Model reduction and physical understanding of slowly oscillating processes: the circadian cycle. *Multiscale Model. Simul.* **5**, 1297–1332.

GOUSSIS, D. A. & VALORANI, M. 2006 An efficient iterative algorithm for the approximation of the fast and slow dynamics of stiff systems. *J. Comput. Phys.* **214**, 316–346.

HADJINICOLAOU, M. & GOUSSIS, D. A. 1998 Asymptotic solution of stiff PDEs with the CSP method: the reaction–diffusion equation. *SIAM J. Sci. Comput.* **20**, 781–810.

JIMENEZ, C. & CUENOT, B. 2007 DNS study of stabilization of turbulent triple flames by hot gases. *Proc. Combust. Inst.* **31**, 1649–1656.

JOEDICKE, A., PETERS, N. & MANSOUR, M. 2005 The stabilization mechanism and structure of turbulent hydrocarbon lifted flames. *Proc. Combust. Inst.* **30**, 901–909.

KALGHATGI, G. T. 1984 Lift-off heights and visible lengths of vertical turbulent jet diffusion flames in still air. *Combust. Sci. Technol.* **41**, 17–19.

KAPER, H. G. & KAPER, T. J. 2002 Asymptotic analysis of two reduction methods for systems of chemical reactions. *Physica D* **165**, 66–93.

KAZAKOV, A., CHAOS, M., ZHAO, Z. W. & DRYER, F. L. 2006 Computational singular perturbation analysis of two-stage ignition of large hydrocarbons. *J. Phys. Chem.* A **110**, 7003–7009.

LAM, S. H. 1985 Singular perturbation for stiff equations using numerical methods. In *Recent Advances in the Aerospace Sciences* (ed. Corrado Casci, in honor of Luigi Crocco). Plenum.

LAM, S. H. 1992 The effects of fast chemical reactions on mass diffusion. *MAE Rep.* T1953, Princeton University, New Jersey.

LAM, S. H. 1993 Using CSP to understand complex chemical kinetics. *Combust. Sci. Technol.* **89**, 375–404.

LAM, S. H. 2007 Reduced chemistry-diffusion coupling. *Combust. Sci. Technol.* **179**, 767–786.

LAM, S. H. & GOUSSIS, D. A. 1994 The CSP method for simplifying kinetics. *Intl J. Chem. Kinet.* **26**, 461–486.

LEE, J. C., NAJM, H. N., LEFANTZI, S., RAY, J., FRENKLACH, M., VALORANI, M. & GOUSSIS, D. A. 2007 A CSP and tabulation-based adaptive chemistry model. *Combust. Theory Model.* **11**, 73–102.

LI, J., ZHAO, Z. W., KAZAKOV, A. & DRYER, F. L. 2004 An updated comprehensive kinetic model of hydrogen combustion. *Intl J. Chem. Kinet.* **36**, 566–575.

LU, T. F., JU, Y. G. & LAW, C. K. 2001 Complex CSP for chemistry reduction and analysis. *Combust. Flame* **126**, 1445–1455.

LU, T. F. & LAW, C. K. 2008 A CSP-based criterion for the identification of QSS species: a reduced mechanism for methane oxidation with no chemistry. *Combust. Flame* **154**, 761–774.

LU, T. F., LAW, C. K. & JU, Y. G. 2003 Some aspects of chemical kinetics in Chapman-Jouguet detonation: induction length analysis. *J. Propul. Power* **19**, 901–907.

MAAS, U. & POPE, S. B. 1992 Simplifying chemical kinetics: intrinsic low-dimensional manifolds in composition space. *Combust. Flame* **88**, 239–264.

MARKIDES, C. N. & MASTORAKOS, E. 2005 An experimental study of hydrogen autoignition in a turbulent co-flow of heated air. *Proc. Combust. Inst.* **30**, 883–891.

MASSIAS, A., DIAMANTIS, D., MASTORAKOS, E. & GOUSSIS, D. A. 1999a Global reduced mechanisms for methane and hydrogen combustion with nitric oxide formation constructed with CSP data. *Combust. Theory Model.* **3**, 233–257.

MASSIAS, A., DIAMANTIS, D., MASTORAKOS, E. & GOUSSIS, D. A. 1999b An algorithm for the construction of global reduced mechanisms with CSP data. *Combust. Flame* **117**, 685–708.

MIZOBUCHI, Y., SHINJO, J., OGAWA, S. & TAKENO, T. 2005 A numerical study on the formation of diffusion flame islands in a turbulent hydrogen jet lifted flame. *Proc. Combust. Inst.* **30**, 611–619.

PETERS, N. & WILLIAMS, F. A. 1983 Liftoff characteristics of turbulent jet diffusion flames. *AIAA J.* **21**, 423–429.

PITTS, W. M. 1988 Assessment of theories for the behaviour and blowout of lifted turbulent jet diffusion flames. *Proc. Combust. Inst.* **22**, 809–816.

REN, Z. & POPE, S. B. 2006 The use of slow manifolds in reactive flows. *Combust. Flame* **147**, 243–261.

REN, Z. & POPE, S. B. 2007a Transport-chemistry coupling in the reduced description of reactive flows. *Combust. Theory Model.* **11**, 715–739.

REN, Z. & POPE, S. B. 2007b Reduced description of complex dynamics in reactive systems. *J. Phys. Chem.* A **111**, 8464–8474.

SINGH, S., POWERS, J. M. & PAOLUCCI, S. 2002 On slow manifolds of chemically reactive systems. *J. Chem. Phys.* **117**, 1482–1496.

SU, L. K., SUN, O. S. & MUNGAL, M. G. 2006 Experimental investigation of stabilization mechanisms in turbulent, lifted jet diffusion flames. *Combust. Flame* **144**, 494–512.

TACKE, M. M., GEYER, D., HASSEL, E. P. & JANICKA, J. 1998 A detailed investigation of the stabilization point of lifted turbulent diffusion flames. *Proc. Combust. Inst.* **27**, 1157–1165.

UPATNIEKS, A., DRISCOLL, J. F., RASMUSSEN, C. C. & CECCIO, S. L. 2004 Liftoff of turbulent jet flames: assessment of edge flame and other concepts using cinema-PIV. *Combust. Flame* **138**, 259–272.

Valorani, M., Creta, F., Goussis, D. A., Lee, J. C. & Najm, H. N. 2006 An automatic procedure for the simplification of chemical kinetic mechanisms based on CSP. *Combust. Flame* **146**, 29–51.

Valorani, M., Goussis, D. A., Creta, F. & Najm, H. N. 2005 Higher order corrections in the approximation of low-dimensional manifolds and the construction of simplified problems with the CSP method. *J. Comput. Phys.* **209**, 754–786.

Valorani, M., Najm, H. N. & Goussis, D. A. 2003 CSP analysis of a transient flame-vortex interaction: time scales and manifolds. *Combust. Flame* **134**, 35–53.

Vanquickenborne, L. & van Tiggelen, A. 1966 Stabilization mechanism of lifted diffusion flames. *Combust. Flame* **10**, 59–69.

Yamashita, H., Shimada, M. & Takeno, T. 1996 A numerical study on flame stability at the transition point of jet diffusion flames. *Proc. Combust. Inst.* **26**, 27–34.

Yoo, C. S., Sankaran, R. & Chen, J. H. 2009 Three-dimensional direct numerical simulation of a turbulent lifted hydrogen/air jet flame in heated coflow: flame stabilization and structure. *J. Fluid Mech.* **460**, 453–481.

Zagaris, A., Kaper, H. G. & Kaper, T. J. 2004a Analysis of the computational singular perturbation reduction method for chemical kinetics. *J. Nonlinear Sci.* **14**, 59–91.

Zagaris, A., Kaper, H. G. & Kaper, T. J. 2004b Fast and slow dynamics for the computational singular perturbation method. *Multiscale Model. Simul.* **2**, 613–638.

Zagaris, A., Kaper, H. G. & Kaper, T. J. 2005 Two perspectives on reduction of ordinary differential equations. *Math. Nachr.* **278**, 1629–1642.